International Journal of Nanomedicine

Dovepress
open access to scientific and medical research

Open Access Full Text Article

ORIGINAL RESEARCH

# Combined Molybdenum Gelatine Methacrylate Injectable Nano-Hydrogel Effective Against Diabetic Bone Regeneration

Xun Liao[1,*], Mingkui Shen[2,*], Tengbo Li[3], Li Feng[3], Zhao Lin[1], Guang Shi[1], Guoxian Pei[3], Xiyu Cai[1]

[1]Department of Orthopedics, The Fifth Affiliated Hospital, Sun Yat-sen University, Zhuhai, Guangdong Province, 519000, People's Republic of China; [2]Henan Provincial Third People's Hospital, Zhengzhou, Henan Province, 450000, People's Republic of China; [3]School of Medicine, Southern University of Science and Technology, Shenzhen, Guangdong Province, 519000, People's Republic of China

*These authors contributed equally to this work

Correspondence: Xiyu Cai; Guoxian Pei, Email caixirain@163.com; nfperry@163.com

**Introduction:** Bone defects in diabetes mellitus (DM) remain a major challenge for clinical treatment. Fluctuating glucose levels in DM patients lead to excessive production of reactive oxygen species (ROS), which disrupt bone repair homeostasis. Bone filler materials have been widely used in the clinical treatment of DM-related bone defects, but overall they lack efficacy in improving the bone microenvironment and inducing osteogenesis. We utilized a gelatine methacrylate (GelMA) hydrogel with excellent biological properties in combination with molybdenum (Mo)-based polyoxometalate nanoclusters (POM) to scavenge ROS and promote osteoblast proliferation and osteogenic differentiation through the slow-release effect of POM, providing a feasible strategy for the application of biologically useful bone fillers in bone regeneration.

**Methods:** We synthesized an injectable hydrogel by gelatine methacrylate (GelMA) and POM. The antioxidant capacity and biological properties of the synthesized GelMA/POM hydrogel were tested.

**Results:** In vitro, studies showed that hydrogels can inhibit excessive reactive oxygen species (ROS) and reduce oxidative stress in cells through the beneficial effects of pH-sensitive POM. Osteogenic differentiation assays showed that GelMA/POM had good osteogenic properties with upregulated expression of osteogenic genes (BMP2, RUNX2, Osterix, ALP). Furthermore, RNA-sequencing revealed that activation of the PI3K/Akt signalling pathway in MC3T3-E1 cells with GelMA/POM may be a potential mechanism to promote osteogenesis. In an in vivo study, radiological and histological analyses showed enhanced bone regeneration in diabetic mice, after the application of GelMA/POM.

**Conclusion:** In summary, GelMA/POM hydrogels can enhance bone regeneration by directly scavenging ROS and activating the PI3K/Akt signalling pathway.

**Keywords:** diabetic bone regeneration, nanomaterials, antioxidation

## Introduction

Bone defects caused by trauma, tumour surgery, or ageing are a serious burden on millions of patients, not only physically but also mentally.[1] The metabolic characteristics of patients with diabetes, characterized by elevated blood glucose levels and systemic inflammation, seriously affect the repair of bone defects, thus making diabetic bone defects a major clinical challenge.[2] Blood glucose fluctuations due to lack of control are commonly observed in patients with diabetes due to refusal to follow medical advice and irregularity of treatment.[3] Numerous experimental studies have found that fluctuations in glucose levels severely affect bone defect repair and may induce metabolic and mitochondrial disorders characterized by oxidative stress damage.[4] Glucose fluctuations in diabetes cause the production of reactive oxygen species (ROS), which exacerbate the inflammatory response and degrade host tissue, thereby creating a proinflammatory microenvironment at the site of the bone defect. This change reduces the function of downstream

Received: 25 July 2023
Accepted: 8 October 2023
Published: 20 October 2023

bone progenitor cells and leads to bone regeneration.[5] Due to the lack of the ability to adjust the diabetic microenvironment (high-level ROS), traditional bone filling materials have difficulty achieving the repair of bone tissue defects. However, the development of new materials and the realization of bone repair through microenvironment remodelling is a new direction in the field of bone tissue engineering.

Numerous studies have shown that diabetes impairs all stages of fracture defect healing in multiple ways, including but not limited to hyperinsulinaemia, obesity and increased bone marrow fat, chronic hyperglycaemia and accumulation of AGEs, inflammation, senescent cell accumulation, diabetic complications such as microvascular disease and neuropathy,[6–8] and an increase in ROS, which suggest a state of excess oxidizing agents.[9] ROS are naturally occurring oxygen-containing molecules produced as a byproduct of cellular metabolism and are important in normal physiological and redox biological reactions.[10] However, elevated levels of ROS inhibit the osteogenic function of osteoblasts, osteocytes, and mesenchymal cells and activate osteoclasts, thereby inducing osteoclastic effects.[11–13] Therefore, the design of bone fillers capable of scavenging excess ROS and maintaining the microenvironment of the bone defect at the bone defect site may help to improve the treatment of bone defects in patients with diabetes.

For treatment of bone defects, autografts, allografts, and xenografts are commonly used in clinical practice. However, these methods cannot be applied on a large scale because of limited donor quality, poor osteogenic induction, susceptibility to infection, host immune response, and suboptimal bioactivity.[14,15] Biomaterial-based tools are increasingly being specifically designed for bone reconstruction but only a few are specifically designed to control the microenvironment of diabetic bone defects. Controlling the microenvironment of diabetic bone defects by reducing reactive oxygen-induced oxidative stress through the administration of reactive oxygen scavengers is an effective method.[16,17]

Molybdenum (Mo)-based polyoxometalate nanoclusters (POM), described as clusters of transition metals (typically referring to W, Mo, V, and Nb) and oxygen atoms and have been used as ROS scavengers to treat inflammation in recent years.[18] In addition, it was reported that the valence state of the Mo ion of POM was found to vary between Mo5+ and Mo6+ when it was reduced or oxidized. POM scavenges ROS by changing the reduction and oxidation state and has been shown to be an effective treatment for many diseases.[19,20] However, the above applications of POM are limited to the direct utilization of the excellent biological properties of POM. We innovatively incorporated it into a hydrogel to make it a slow-release and precise treatment for diabetic bone defects.

Various types of bone-filling materials, including metals, ceramics, and polymers, have been extensively studied.[15] However, hydrogels, which mimic the extracellular matrix (ECM) and provide a hydrophilic three-dimensional microenvironment suitable for endogenous cell growth, are attracting increasing attention.[21] Gelatine methacrylate (GelMA) is a seminatural synthetic hydrogel. Its high biocompatibility and abundant pores allow freer movement of substances in and out.[22] Due to the grafting of MA, GelMA is malleable and shows sustained release under visible light curing.[23] However, previous research on hydrogels has focused more on their physicochemical properties for better biocompatibility and cellular response properties, such as providing suitable cell adhesion sites and enhancing protein hydrolytic degradability and adhesion, ignoring their biological effects on the tissue microenvironment.[24,25] However, injectable hydrogels with antioxidant properties were prepared by combining GelMA and POM, which not only possessed excellent physicochemical properties but also had biological effects by improving the tissue microenvironment.

P13K refers to Phosphoinositide 3-kinase, a family of Kinase enzymes that recruit and activate the Akt kinase, also known as Protein Kinase B, which acts on multiple signaling molecules when Akt is activated. And the PI3K/Akt signalling pathway has been found to play an important role in cell growth, reproduction and differentiation.[26] In addition, previous studies have revealed that PI3K/Akt is an important signalling pathway that regulates bone repair, which can regulate the differentiation of osteoclasts and osteogenic differentiation.[27]

In this study, we developed an injectable hybrid hydrogel with antioxidative properties by encapsulating POM into GelMA. The hydrogel has a space suitable for cell growth and differentiation and a pore structure conducive to material exchange, and has good adhesion and degradability. POM is released at the bone defect and persistently scavenges excess ROS. In vitro, experiments evaluated whether the GelMA/POM hydrogel has good bone-enabling properties under oxidative stress conditions. In addition, to explore the potential molecular mechanism of GelMA/POM hydrogel to promote osteogenesis, we performed RNA sequencing. Then, the hydrogel was injected into a diabetic mouse model of a distal femoral defect to observe its effect on the repair of bone defects. The injectable antioxidant hydrogel is expected to

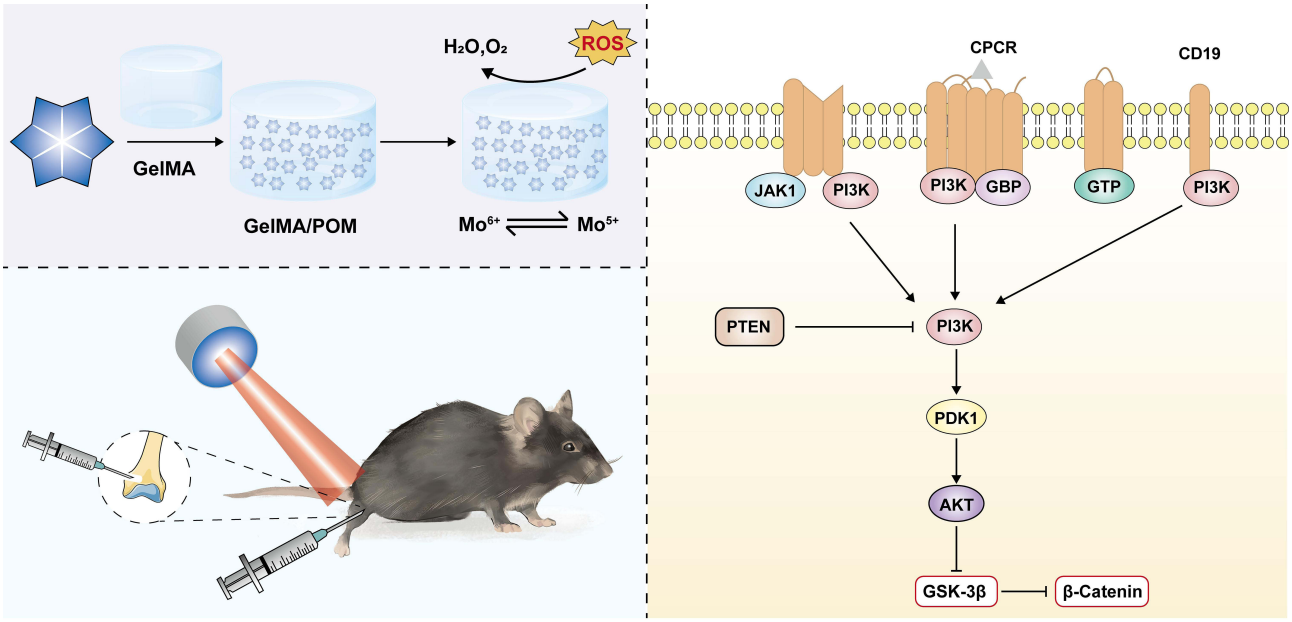


**Scheme 1** Schematic illustration of synthetic GelMA/POM hydrogel induction of bone defect repair and the mechanism of osteogenic induction.

be a bone filling material with the ability to adjust the diabetic microenvironment for the repair of bone defects in diabetic patients (Scheme 1).

# Materials and Methods

## Synthesis of Polyoxometalate Nanoclusters (POM)

Molybdic acid ammonium salt ($(NH4)_6Mo_7O_{24}\cdot 4\ H_2O$ (5.00 g)) was dissolved in 20 mL of $ddH_2O$ at 25 °C under continuous agitation, followed by rapid addition of adding 5 mL of $ddH_2O$ containing 1.17 mmol of $NaH_2PO_4$. Subsequently, another 4 mL of saturated L-ascorbic acid was dripped into the system and agitated for 10 min. Then, the polyoxometalates were precipitated by adding 100 mL of ethanol, and collected by centrifugation at 12,000×g for 15 min. After the precipitate was dried in a vacuum desiccator for 72 h to completely eliminate ethanol, POM was obtained and stored for future research.

## Synthesis of Hydrogels

Gelatine methacrylate (GelMA) (molecular weight = 150,000) (EFL-GM-50, Engineering for Life, China) is a white spongy powder. GelMA was added to a solution equipped with lithium phenyl-2,4,6-trimethylbenzoylphosphonate (LAP) and PBS and mixed well. The mass concentration of LAP was 0.25%, and the mass concentration of GelMA solution obtained was 6%.

For sterility, the GelMA solution was filtered into a shading container by using an injection filter with aperture size of 0.22 μm and stored at 4 °C. When the experiment demanded, the solution was exposed to blue–violet light (405 nm) for approximately 10s. For GelMA/POM hydrogels, the GelMA solution was mixed evenly with POM and then exposed to blue–violet light (405 nm) for approximately 10s.

## Characterization of Polyoxometalate Nanoclusters (POM)

Images were taken with an FEI Tecnai 20 transmission electron microscope (TEM). The size of the POM in the TEM image was measured using ImageJ software. A microscope acceleration voltage of 200 kV was used. X-ray photoelectron spectroscopy (XPS) measurements of POM were carried out before and after being completely oxidized by ROS (ie, $H_2O_2$). The pH of this oxidation was 7.5. XPS observation was carried out on a Thermo Scientific KAlpha, operating at an Al target of 1486.6 eV. The full spectrum pass energy was 100 eV, and the step size was 1.0 eV.

## Characterization of Gelatine Methacrylate (GelMA) and Gelatine Methacrylate / Polyoxometalate Nanoclusters (GelMA/POM) Hydrogels

The microstructures of the GelMA and GelMA/POM hydrogels were further investigated by SEM. The samples were prepared as before and the hydrogels were processed using a freeze dryer (Alpha 1–2LD plus, Christ, Germany) before SEM analysis at 12.5 kV.

Release assays: The hydrogel was made into a cylindrical sample with a diameter of approximately 8 mm and a thickness of 4 mm. The samples were then immersed in PBS for 1, 3, 5, 7, 10, and 14 days at 37 °C at an even pace on a shaker. Finally, at each of the above time points, the supernatant was collected and examined by absorbance measurement (Infinite 200 Pro, Tecan, Switzerland) and compared with the standard curve.

The total antioxidant capacity (TAOC) of POM, GelMA, and GelMA/POM (according to the synthesis method described above) was then tested. The TAOC was determined by using the Total Antioxidant Capability Test Kit (BC1315, Solarbio, China) according to the manufacturer's introductions. POM, GelMA, and GelMA/POM were placed into a 96-well plate followed by the TAOC test kit reagent. After reaction for 10 minutes at room temperature, the absorbance of the reaction solution was detected at 593 nm and compared with the standard curve.

## In vitro Cell Biocompatibility Measurements

Preosteoblast MC3T3-E1 cells were obtained from Procell Bioscience (China). The cell culture medium was complete growth medium containing DMEM, 10% foetal bovine serum (Gibco), and 1% penicillin/streptomycin. The cells were cultured in an incubator with an atmosphere of 5% $CO_2$ at 37 °C. After 80% confluence, these cells were passed into new culture dishes. Before the cell culture work, the solution of nanoparticles was filtered into the test tube by an injection filter with an aperture size of 0.22 μm, and the hydrogel was then prepared and placed in DMEM at 37°C overnight. MC3T3-E1 cells were seeded into a 96-well plate. Then, the medium containing the POM gradient concentration (0, 75 μg/mL, 150 μg/mL, 300 μg/mL, 600 μg/mL, and 1200 μg/mL) was used for 1 and 3 days of incubation. After incubation with 10 μL of CCK-8 solution (C0038, beyotime, China), the absorbance was tested using a microplate reader at 450 nm. Moreover, the preosteoblasts were grown on various hydrogels separately and cultured, and the CCK-8 assay was performed as described above.

MC3T3-E1 cells were inoculated at a density of 100,000 cells per well on the surface of GelMA and GelMA/ POM hydrogels in 24-well plates and cultured in an incubator. After a period of cultivation, cells adhering to the surface of the hydrogel were washed with PBS. Then, the cells were fixed with 4% paraformaldehyde (PFA) (P0099, beyotime, China) for 15 minutes, followed by infiltration with 0.1% (v/v) Triton X-100 for 10 minutes. Finally, AbFluor™ 488-Phalloidin (Abbkine, China) was used to stain cellulars F-actin for 30 minutes, and DAPI was used to stain cell nuclei for 10 minutes. The morphology of the cells was observed through a confocal fluorescence microscope (Nikon, Japan). Furthermore, a live/dead cell imaging kit (R37601, Invitrogen, USA) was used to evaluate both live and dead MC3T3-E1 cells. Next, the labelled cells were observed through laser scanning confocal microscopy (LSCM, Nikon, Japan) and then analysed with ImageJ. Cell viability was calculated as follows: Cell viability (%) = (number of live cells/ total number of cells) × 100%.

## In vitro Antioxidant Assay

Antioxidant capacity in cells: MC3T3-E1 cells were inoculated at a density of 1,000,000 per well in a 6-well plate. After treatment with 100 μM $H_2O_2$ for 20 min, 300 μg/mL POM was added to the well. After 1 day of incubation, the ROS level was examined with the corresponding reactive oxygen species assay kit (CA1410, Solarbio, China) based on the manufacturer's introductions.

MC3T3-E1 cells incubated with $H_2O_2$ were seeded into a 6-well plate. When the cells were about to grow to full size, a 1000 μL pipette tip was used to scratch the cell monolayer, and the cells were photographed using a microscope. After 24 h of incubation with medium containing low concentrations of serum, the cells were photographed again using a microscope. The migration of the cells was derived by comparative analysis of the scratched areas before and after scratching areas using ImageJ software. For evaluation of the viability and morphology of the cells attached to the hydrogel, MC3T3-E1 cells were inoculated at a density of 100,000 cells per well on the GelMA and GelMA/POM

hydrogel surfaces of 24-well plates. After a period of cultivation, cells adhering to the surface of the hydrogel were washed with PBS. Then, the cells were fixed with 4% paraformaldehyde (PFA) for 15 minutes, followed by infiltration with 0.1% (v/v) Triton X-100 for 10 minutes. Finally, cell live-death experiments were performed and cell morphology were studied as described above.

## In vitro Osteogenic Differentiation Assays

MC3T3-E1 cells were treated with osteogenic media containing DMEM with 10% FBS, 1% PS, 10 mM b-glycerol phosphate (G9422, Sigma-Aldrich, Germany), 0.1 mM dexamethasone (D4902, Sigma Aldrich, Germany), and 300 mM ascorbic acid (A4403, Sigma-Aldrich, Germany) in the presence of GelMA or GelMA/POM. After culture for 14 days, the cell suspension was obtained by dissolving the hydrogel. Then the collected cells were lysed by RIPA buffer (89,900, Thermo Fisher, US), and the cell supernatant was collected. For analysis of ALP activity, cell lysates were incubated with ALP kit substrate (P0321S, Beyotime, China) for 30 minutes at 37 °C, followed by detection of absorbance at 405 nm using a microplate reader. Finally, ALP activity levels were calculated according to the instructions in the ALP kit. For ALP staining, the cells were collected by the above method and cultured for 24 h. Then, ALP was stained by using an alkaline phosphatase assay kit (C3250S, Beyotime, China). Mineralized nodules were observed by Alizarin Red staining (ARS) (C0148S, Beyotime China). ARS staining results were captured by microscopy. Then the mineralized nodules formed during osteogenic differentiation were dissolved in cetylpyridinium chloride (10 mmol/L) (C798322, Macklin, China) for 30 min. Then, 100 L of supernatant from different groups was added to a 96-well plate, and the absorbance at 570 nm was measured using a microplate reader. The optical density (OD) was analysed.

## RNA-Sequencing Analysis

Cells from the GelMA group and GelMA/POM group were collected after 7 days of culture in osteogenic differentiation medium. The total RNA of MC3T3-E1 cells was extracted by using an RNA column extraction kit (Vazyme, China). Samples were then tested for purity using a NanoPhotometer spectrophotometer (Thermo Fisher). Transcriptome sequencing technology and methods were provided by Annoroad Gene Technology, and sequencing was performed using the Illumina sequencing platform. For screening of differentially expressed genes (DEGs), the selection criteria were $|\log FC|>1$ and $P<0.05$. For further analysis of expressed genes, both Gene Ontology (GO) analysis of the sequence information of genes and Kyoto Encyclopedia of Genes and Genomes (KEGG) analysis of the expression information of genes were used.

## Quantitative Real-Time PCR (qRT–PCR)

The expression levels of osteogenic genes (ALP, BMP2, Osterix and Runx2) and PI3K/Akt signalling factors (PTEN, GSK-3β and β-catenin) were assessed by qRT–PCR analysis. Briefly, cells ($5 \times 10^4$ cells/well) were seeded on the surface of the hydrogel in 6-well tissue culture plates. After osteogenic induction, total RNA was extracted from cells using a Cell/Tissue Total RNA Isolation Kit and then reverse transcribed into cDNA by a cDNA transcription kit (R312-01, Vazyme, China) on Day 7. Afterwards, qRT–PCRs were performed on an ABI Step One Plus Real-Time PCR system (Applied Biosystems, USA) using Taq Pro Universal SYBR qPCR Master Mix (Vazyme, China). Finally, the relative expression of each gene was normalized to that of the housekeeping gene glyceraldehyde-3-phosphate dehydrogenase (GAPDH). The gene primers are listed in Table 1.

## In vivo Bone Regeneration of Hydrogel

The effect of this hydrogel on bone regeneration in vivo was further investigated by constructing a distal femoral defect model. All work performed on animals was approved by the Animal Ethics Committee of the Fifth Affiliated Hospital of Sun Yat-sen University (00347) according to laboratory animal-Guideline for ethical review of welfare and conducted in accordance with the Guide for the Care and Use of Animals for research purposes. Diabetes was induced by injecting eight-week-old female C57BL/6 mice intraperitoneally with 50 mg/kg body weight streptozotocin (STZ; S8050, Solarbio, China) dissolved in citrate buffer (pH 5.5) for 5 days. Animal fasting weight and tail vein blood glucose concentrations were measured 2 weeks after STZ administration. Only STZ-injected mice with fasting blood glucose

**Table 1** Primers for Real-Time PCR

| Gene | Forward Primer (5′-3′) | Reverse Primer (5′-3′) |
|---|---|---|
| RUNX2 | CCAACTTCCTGTGCTCCGTG | ATAACAGCGGAGGCATTTCG |
| ALP | GCACTGCCACTGCCTACTT | AGCTGATATGCGATGTCCTT |
| BMP2 | ATGTGAGGATTAGCAGGTCTTTG | TGGTTAGTGGAGTTCAGGTGGT |
| Osterix | TGACTACCCACCCTTCCCTC | GCCTTGTACCACGAGCCATA |
| GSK-3β | GACTTTGGAAGTGCAAAGC | AGGAAATATTGGTTGTCCTAGC |
| PTEN | CAAAGCAAACAAAGACAAGGCC | CTCTGGATTTGATGGCTCCTCTAC |
| β-Catenin | ATGGAGCCGGACAGAAAAGC | CTTGCCACTCAGGGAAGGA |
| GAPDH | AGCTTCGGCACATATTTCATCTG | CGTTCACTCCCATGACAAACA |

concentrations >11.1 mmol/l were used as the experimental study object. Then, the induced C57/BL6-mice were divided into three groups (control, GelMA, and GelMA/POM, n=8).

Mice were fasted overnight prior to surgery, and water intake was restricted, which reduced intraoperative excretion. The mice were anaesthetized by inhalation of isoflurane gas, and after successful anaesthesia, the mice were fixed in a prone position on the operating table. After removal of the surgical site hair and disinfection of the surgical field from the inside out with iodine swabs, meloxicam (0.1 mg/kg) was injected subcutaneously for pain management, a surgical incision of approximately 1 cm was made at the distal femur, and blunt separation of subcutaneous fat and muscle was performed to expose the distal femur. The bone defect was generated using an electric drill with a 1-mm diameter drill bit. After injection of sterilized GelMA or GelMA/POM solution, irradiation with blue light for 10s was performed for adherence to the defect. The wound was closed with surgical silk sutures. Intramuscular penicillin sodium (4 IU/kg) and subcutaneous meloxicam (0.1 mg/kg) were administered daily for 3 days after surgery. The mice were euthanized at the 2nd and 4th postoperative weeks, and distal femur specimens were taken and fixed in 4% PFA for 2 days, and then scanned with micro-CT (SkyScan 1276, Bruker, Belgium) at 60 kV and 100 mA. Data were processed using NRecon, CTAn, and CTvol software The data were processed and 3D images were reconstructed using NRecon, CTAn, and CTvol software. Bone mineral density (BMD) and bone volume fraction (calculated as a percentage of bone volume to tissue volume (BV/TV)) were also analysed for each group of mice. Isolated femoral specimens were fixed in 4% PFA for 2 days and then transferred to EDTA decalcification solution (GCND0078, OKA, China) for shaking and decalcification for 3 weeks. The samples were then dehydrated and embedded in paraffin and sent to the microtome for paraffin sectioning. Haematoxylin and eosin (H&E) staining was performed to further evaluate the new bone tissue in the defect area. Finally, a scanner (Leica, Germany) was used to obtain digital images of the sections.

## Statistical Analysis

Statistical analysis was carried out with GraphPad Prism 8.0 software. Data were recorded as the mean ± SEM. Student's *t*-test was used to evaluate the statistical significance of differences between two groups. The statistical significance of differences among multiple groups was determined by one-way ANOVA for multiple comparisons. For all tests, p value <0.05 was considered to indicate statistical significance.

# Results and Discussion

## Characterization of Polyoxometalate Nanoclusters (POM)

Figure 1A shows the TEM image of POM, which indicated that POM exhibited an average diameter of 1–2 nm (Supplement Figure 1). The small size of the nanomaterial results in a relatively large specific surface area and easy ion release, which is conducive to the dissolution of the nanomaterial in solvents.[28] POM exhibited high $H_2O_2$ scavenging activity, and its blue colour bleached when $H_2O_2$ was added (Figure 1B). The potent ROS scavenging performance of POM originated from the electron transfer between Mo5+ and Mo6+ ions,[29] which was further confirmed by XPS (Figure 1C).

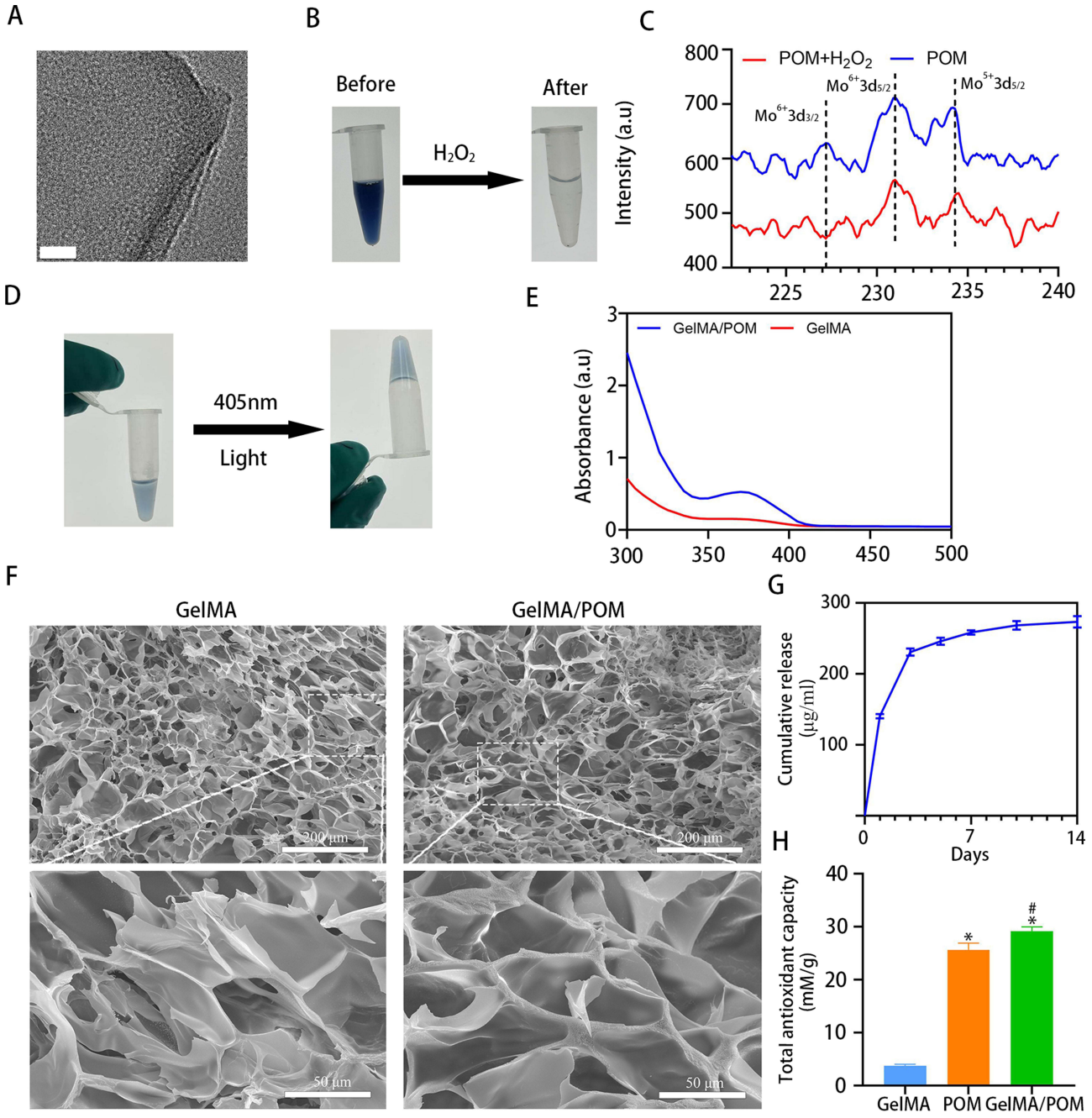


**Figure 1** Characterization of POM and GelMA/POM hydrogel. (**A**) POM images were taken at pH = 7.5 by TEM; scale bar: 20 nm. (**B**) POM before and after incubation with $H_2O_2$. (**C**) X-ray photoelectron spectroscopy of POM incubating with or without ROS. (**D**) GelMA/POM before and after blue light exposure. (**E**) Surface plasmon absorption of mixed solution with POM and GelMA. (**F**) SEM images of GelMA and GelMA/POM hydrogel. (**G**) Amount of cumulative released POM. (**H**) The total antioxidant capacity of GelMA, POM and GelMA/POM. (*And #Indicate $p < 0.05$ in comparison with the GelMA and POM group, respectively.).

## Characterization of Gelatine Methacrylate/Polyoxometalate Nanocluster (GelMA/POM) Composite Hydrogels

GelMA has been widely used as a filler in tissue repair due to its excellent biocompatibility, degradability, and light-curing ability. In this study, a hybrid hydrogel with the ability to scavenge ROS to adjust the microenvironment of bone defects was synthesized by combining GelMA and POM.[18,30] GelMA/POM was exposed to blue light (405 nm) for 10s. GelMA/POM was quickly converted from a liquid to a hydrogel (Figure 1D). The UV spectra of the GelMA/POM composite showed a strong absorption at 370 nm due to the surface plasmon absorption of POM (Figure 1E), while no absorption was observed for the gelatine solution. SEM revealed that both pure gel hydrogel and hybrid hydrogel had

sponge-like pore structures that were interconnected and uniform (Figure 1F). The large pore structure of hydrogels gives hydrogels good biocompatibility and biosafety in biological applications.[31] As determined by UV spectrophotometry and compared with the concentration standard curve of POM (Supplement Figure 2), the release curve of the GelMA/POM composite hybrid hydrogel was plotted. According to the release curve of the GelMA/POM hydrogel (Figure 1G), the release of POM was mainly concentrated in the first 3 days, leading to a rapid increase in POM concentration. Then, the drug continued to be release for two weeks. The absorbance concentration curve of POM is shown in Supplement Figure 2 and Supplement Figure 3. This phenomenon may be related to the expansion of pore size in the first three days caused by swelling of the hydrogel (Supplement Figure 4). Divband et al believed that the higher the degree of swelling of a hydrogel in an aqueous solution, and the larger the pores formed, and the faster the release of its contents.[32] To further investigate the ability of nanomaterials and hydrogels to scavenge oxidative stress molecules, we conducted experiments on the total antioxidant capacity. The experimental results showed that the POM group had a higher antioxidant activity than the GelMA group, and the GelMA/POM group had the highest total antioxidant capacity (POM concentration: 1 mg/mL) (Figure 1H). This finding indicates that the antioxidant capacity was mainly from POM nanomaterials. Thus, POM can be used as an ROS scavenger by combining with GelMA, giving hydrogels the ability to remove ROS activity.[33] As shown in Supplement Figure 5, the degradation rates were almost the same for all groups at the same time and increased gradually with time. The degradation rate is an important property for a bone-filling material. Ideally, the degradation of the bone filler material should be coordinated with the rate of bone tissue regeneration after implantation of the biomaterial into the patient's bone tissue defect. A rate of degradation of the filler that is too low prevents the repair of new tissue to the defective centre, while a rate of degradation that is too high prevents cells from settling and proliferating.[34,35] The degradation mechanism of GelMA was found to include mainly the hydrolysis reaction of short ions in GelMA and degradation by matrix metalloproteinases (MMPs) secreted by cells.[36,37]

## Biocompatibility of Polyoxometalate Nanoclusters (POM)

POM has an excellent antioxidant capacity, but further determination of the dose of POM in GelMA/POM hydrogels is still needed. There was no significant difference in the growth of MC3T3-E1 cells after addition of different concentrations of POM (0, 75 μg/mL, 150 μg/mL, 300 μg/mL, 600 μg/mL, and 1200 μg/mL) after 1 day and 3 days (Figure 2A). This result indicated the superior biocompatibility of POM with preosteoblastic properties. Therefore, we selected the moderate concentration (300 μg/mL) as the working concentration, which is also close to the concentrations used in previous studies of POM.[18,20] The biocompatibility of different hydrogels was examined by CCK-8 assays, and live/dead and phalloidin staining to determine whether there were differences compared to the blank group. The proliferation of MC3T3-E1 cells seeded on hydrogel was evaluated by CCK-8 assays on the 1st, 3rd and 5th days, as shown in Figure 2B. Although the proliferation of cells grown in the hydrogel was lower than that of the blank control group, the difference between the three groups was not statistically significant. Excellent cell proliferation provides more initial cells and more possibilities for osteogenic differentiation of cells; Thus, good cell proliferation provides the basis for osteogenic differentiation. In addition, almost no dead cells seeded on the hydrogel were observed in the control, GelMA, and GelMA/POM groups after 3 days of culture (Figure 2C and D). No significant differences in cell morphology and nuclei were found among the control, POM and GelMA/POM groups (Figure 2E). In summary, the GelMA/POM hydrogel had good biocompatibility.

## Gelatine Methacrylate / Polyoxometalate Nanocluster (GelMA/POM) Hydrogels Scavenge ROS to Protect Cells

Mitochondria are the centre of oxidative metabolism in cells, and mitochondrial disruption leads to elevated cytoplasmic ROS production. ROS act as redox messengers and regulate cell growth and proliferation. Excess ROS can lead to cell damage affecting cell proliferation.[38] Reactive oxygen species are produced at the site of diabetic bone defects and impede bone regeneration by causing oxidative stress damage to bone tissue and cells at the site of injury. We examined the intracellular ROS levels in each group, and the results are shown in Figure 3A and B. The green fluorescence intensity was enhanced after $H_2O_2$ treatment, indicating an increase in intracellular ROS. The green fluorescence

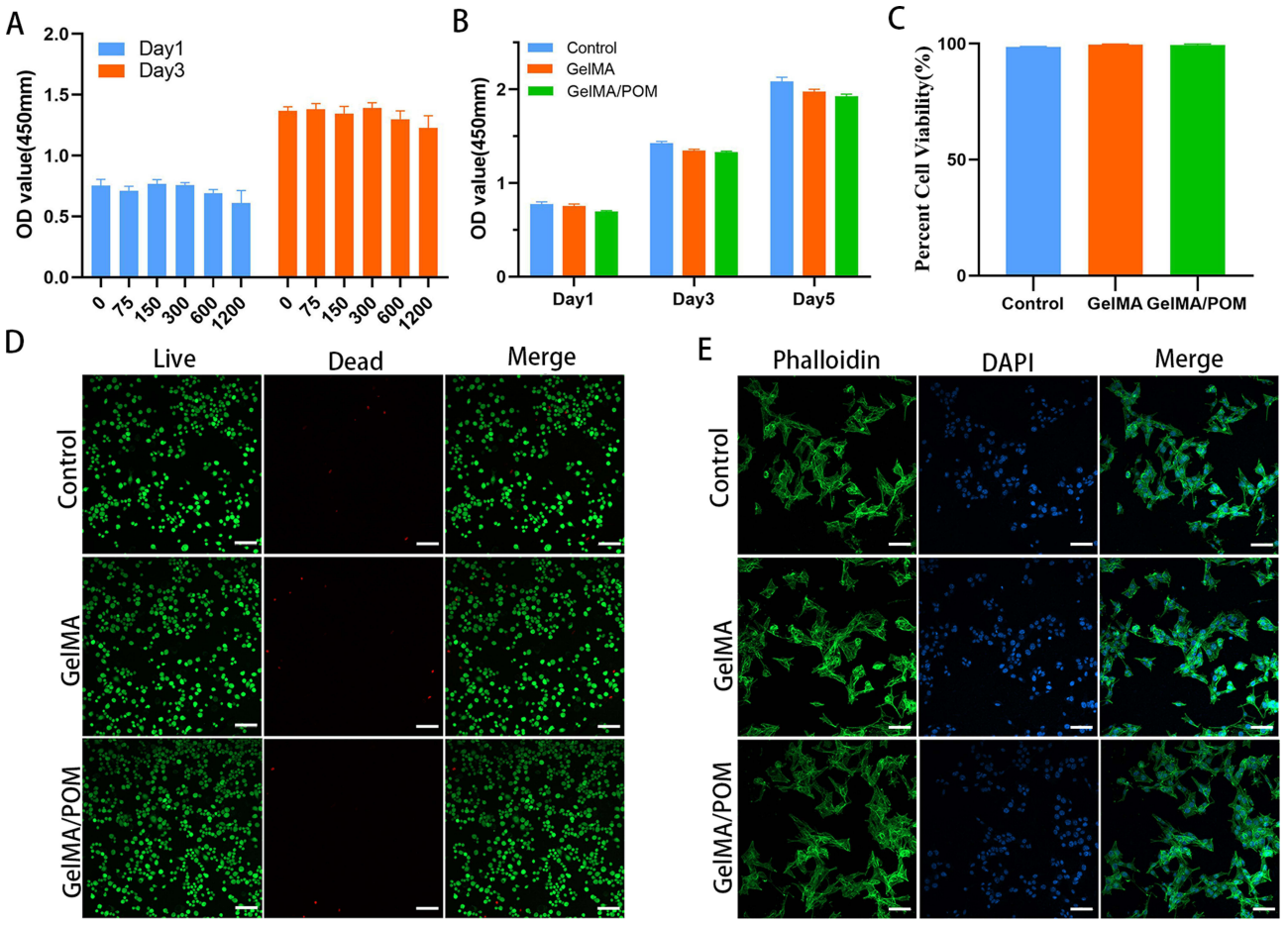


**Figure 2** Cytocompatibility of POM and GelMA/POM hydrogel. (**A**) Cell survival was analyzed at different POM concentrations by using the CCK8 kit. (**B**) The CCK8 assay showing proliferation behavior of MC3T3-E1 cultured on different hydrogels. (**C**) Quantitative analysis of live cells. (**D**) Live/dead staining of cells on the different hydrogels after 3 days of incubation. (**E**) LSCM images of cytoskeleton and nuclei, showing the MC3T3-E1 cells cultured on the surface of the different hydrogels. (n = 3, each group). (Control, cells cultured on the tissue culture plate). Scale bar: 100 μm (**D**), and 100 μm (**E**).

intensity in the GelMA group did not change significantly compared with that in the $H_2O_2$ group, and the green fluorescence in the GelMA/POM group was weakened, which indicated that POM in the GelMA/POM group could act as an ROS scavenger and could reduce the intracellular ROS level. In addition, the results of cell migration experiments are shown in Figure 3C and D. The results indicated that the cell migration of the GelMA/POM group was minimally affected in the oxidative stress environment. Previous studies have shown that the migratory ability of osteoblasts not only determines their localization and distribution in bone tissue but also influences the rate and extent of osteogenic differentiation.[39] Osteoblasts need to migrate to reach the site of bone tissue production or repair, and participate in the synthesis of bone matrix and the ossification process. Osteoblasts release a series of signalling molecules during migration, for example, extracellular calcium signalling molecules released by osteoblasts can promote osteoblast differentiation and ossification.[40] It has been suggested that the cell migration of osteoblasts is an important basis in the process of bone formation.[41] The results of the live-dead experiment are shown in Figure 3E. There were more green-labelled cells in the GelMA/POM group and the POM group, which indicates that there were more live cells. Likewise, the activity of MC3T3-E1 cells grown on GelMA/POM was found to be significantly higher based on quantitative analysis of green-labelled fluorescent cells in live-dead staining (Figure 3F). In addition, cells in the blank control and hydrogel groups were treated with $H_2O_2$, and then, the cytoskeleton was observed using LSCM (Figure 3G). $H_2O_2$-treated MC3T3-E1 cells were spindle-shaped with messy F-actin filaments, whereas cells in the group with the ROS scavenger POM dispalyed actin fibres and a typical fibroblast shape. This finding suggests that the GelMA/POM

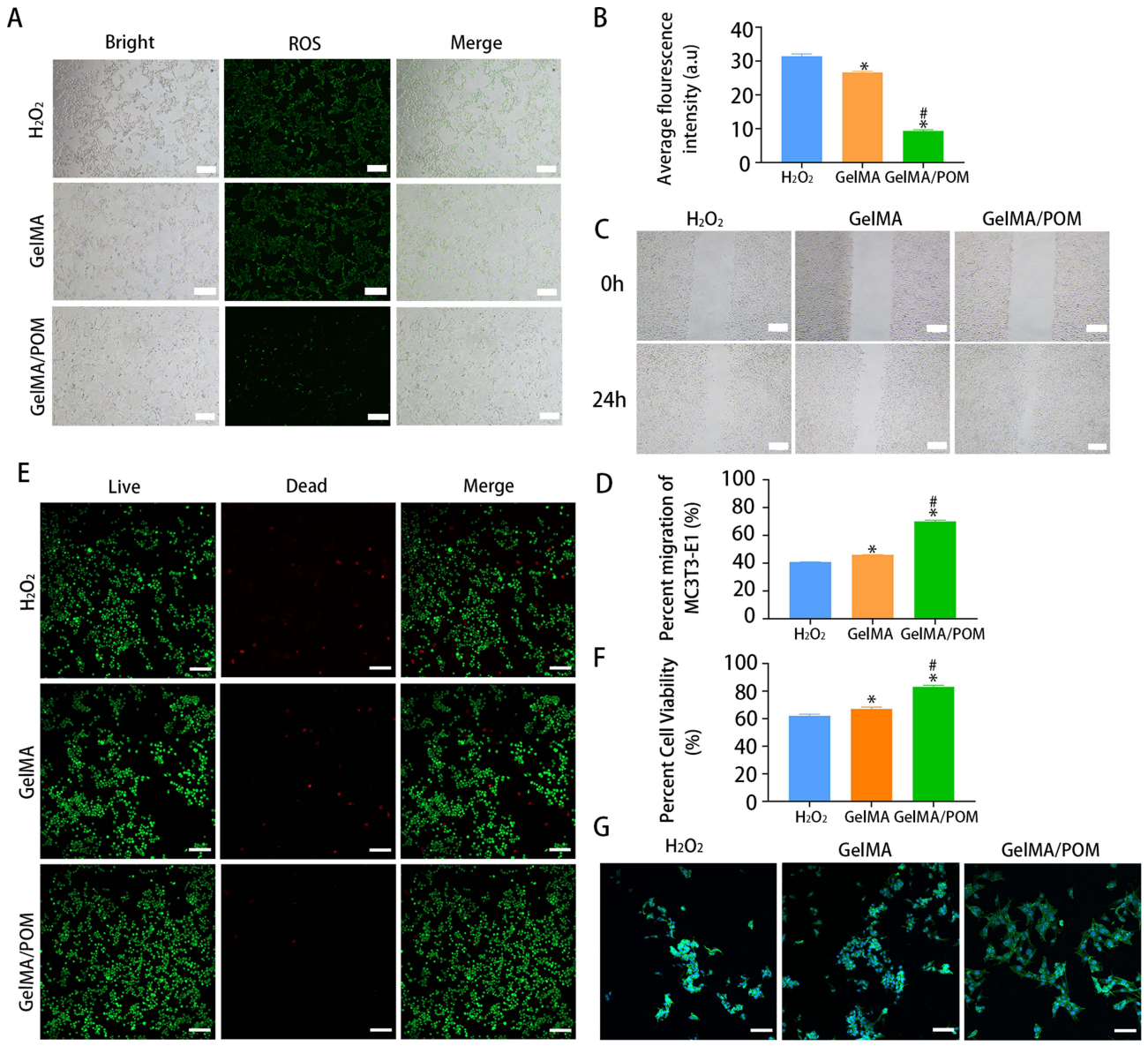


**Figure 3** Antioxidant properties of POM or hydrogel. (**A**) DCFH-DA assay showing intracellular ROS of MC3T3-E1 after incubation with POM in the presence of $H_2O_2$ (100 μM). (**B**) Quantification analysis of DCFH-DA staining (*And #Indicate $p < 0.05$ in comparison with the $H_2O_2$ group and GelMA group, respectively.) (**C**) Cell capacity of migration (scratch test). (**D**) Quantitative analysis of percent migration in scratch assay. (*And #Indicate $p < 0.05$ in comparison with the $H_2O_2$ group and GelMA group, respectively.) (**E**) Live/dead staining showing MC3T3-E1 cell viability after culturing on hydrogel in the presence of $H_2O_2$. (**F**) Quantification analysis of live cells. (*And #Indicate $p < 0.05$ in comparison with the $H_2O_2$ group and GelMA group, respectively.) (**G**) LSCM images showing MC3T3-E1 cultured on different hydrogels following $H_2O_2$ treatment. (n = 3, each group). ($H_2O_2$, cells cultured on the tissue culture plate with $H_2O_2$). Scale bar: 200 μm (**A**), 200 μm (**C**), 100 μm (**E**) and 100 μm (**G**).

hydrogel scavenges ROS via POM, protects cells from high ROS levels in the diabetic microenvironment, prevents oxidative stress damage, and thus accelerates bone regeneration.

## Gelatine Methacrylate / Polyoxometalate Nanoclusters (GelMA/POM) Protect MC3T3-E1 Cells from Osteogenic Differentiation at High ROS Levels

The excellent osteogenic differentiation ability of osteoblasts is essential to promote bone regeneration.[42] Previous studies have shown that high ROS levels prevent osteogenic differentiation of the osteoblasts and that reducing oxidative stress levels promotes osteogenic differentiation.[43] For further analysis of the effect of GelMA/POM on the osteogenic differentiation of MC3T3-E1 cells, in addition to Alizarin Red S staining, Alkaline Phosphatase activity and ALP

staining were also performed. After 14 days of osteogenic induction, the GelMA/POM group had more red staining of calcified nodules than the other $H_2O_2$-treated groups (Figure 4A). And the results of quantitative analysis of calcified nodules were also consistent with the observed results (Figure 4B). A similar effect was observed with ALP activity after 7 days of osteogenic induction. The GelMA/POM group showed significantly higher ALP activity than the other $H_2O_2$-treated group (Figure 4C). For ALP staining, the GelMA/POM group had more ALP-positive cells and darked staining than the other $H2O_2$-treated groups (Figure 4D). The results indicate that the GelMA/POM hydrogel protects osteoblasts and reduces their oxidative stress damage, thereby promoting osteoblast differentiation in a high-ROS environment.

Seven days after MC3T3-E1 underwent osteogenic induction, total cellular RNA was extracted from the GelMA group and GelMA/POM group and analysed by RNA sequencing. Figure 5 shows the results of the RNA sequencing analysis. The volcano plot suggests that GelMA/POM upregulated 1579 DEGs and downregulated 3712 DEGs, which indicates that GelMA/POM altered gene expression in MC3T3-E1 cells with high ROS levels (Figure 5A). In addition, GO statistical analysis (Figure 5B) showed suggestive upregulation of gene expression associated with various biological processes (metabolic process, response to stimulus, and biological regulation). Previous studies have found that promoting cellular metabolic processes may increase osteoblast activity by promoting bone matrix synthesis.[44] In addition, increased cellular

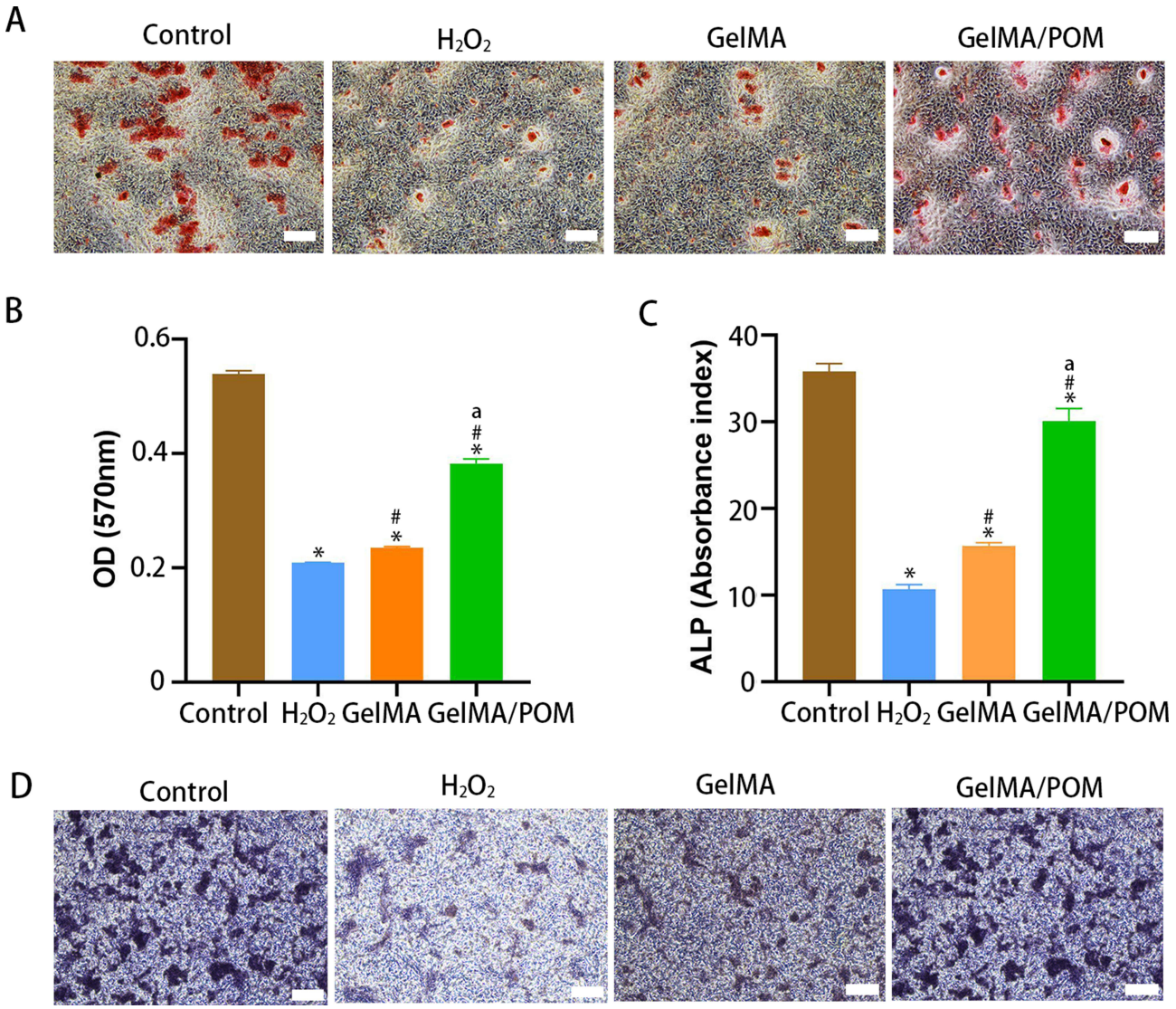


**Figure 4** The osteogenesis properties of GelMA/POM hydrogel in vitro. In vitro assay of effects of hydrogel on ALP activity and extracellular calcium nodule production during osteogenesis differentiation of MC3T3-E1. (**A**) Alizarin red S staining. (**B**) Quantitative analysis of mineralized nodules. (**C**) Alkaline phosphatase activity. (**D**) Alkaline phosphatase staining. (*,# And [a] indicate $p < 0.05$ in comparison with the Control group, $H_2O_2$ group and GelMA group respectively). (Control, cells cultured without $H_2O_2$). (n = 3, each group). Scale bar: 200 μm (**A**) and 200 μm (**D**).

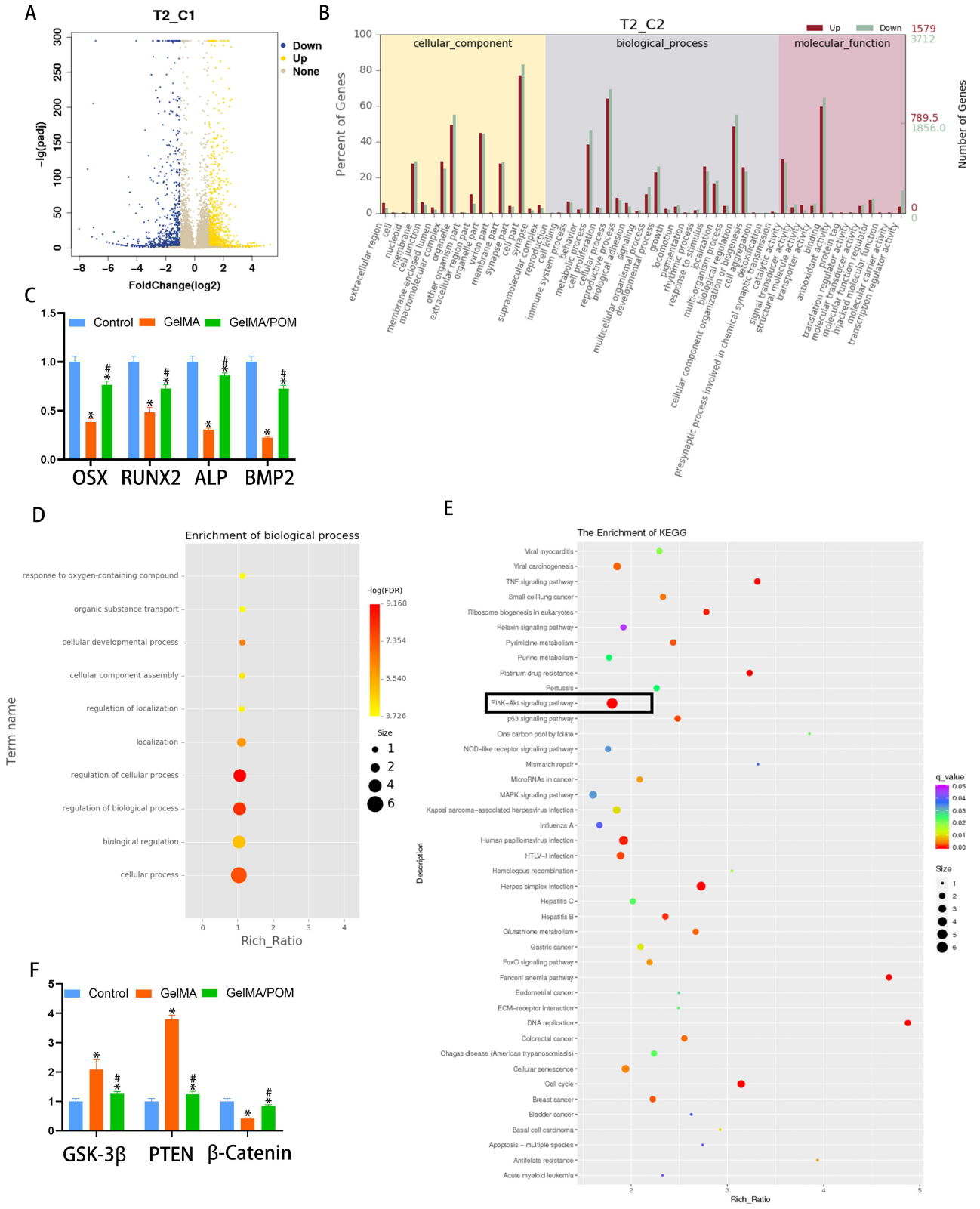


**Figure 5** Transcriptome analysis of the GelMA/POM hydrogel to promote bone repair. (**A**) The differentially expressed genes in GelMA/POM group compared to GelMA group. (**B**) GO analysis of differentially expressed genes between the two groups. (**C**) mRNA levels of the osteogenesis-related genes RUNX2, BMP2, Osterix, and ALP, as determined by real-time PCR. (**D**) Q-value enrichment map of GelMA/POM. The enrichment ratio was calculated as (differentially expressed genes in this pathway/all differentially expressed genes)/ (genes annotated to this pathway/all annotated genes). (**E**) KEGG enrichment analysis of GelMA/POM group compared with GelMA group. (Rectangular box highlights significant differential expression genes.) (**F**) Relative mRNA levels of the PI3K/Akt signaling factors β-catenin, PTEN and GSK-3β, as determined by real-time PCR. (*And #Indicate $p < 0.05$ in comparison with Control group and GelMA group, respectively.) (n = 3, each group).

sensitivity to stimuli and modulation of bioregulatory processes may enhance the cellular response to differentiation signals.[45] This hypothesis was confirmed by qRT–PCR analysis, and GelMA/POM protects cells under oxidative stress and reduces the inhibitory effect of oxidative stress on osteogenic gene(RUNX2, BMP2, Osterix and ALP mRNA) expression.(Figure 5C) BMP2 is a bone morphogenetic protein involved in the differentiation of osteoblast stem cells through activation of intracellular signalling pathways.[46] Osterix and RUNX2 are key transcription factors in bone development and osteogenic differentiation that synergistically regulate osteoblast formation.[47] The above genes synergistically regulate the differentiation, proliferation and function of osteoblasts, which affects bone formation and growth. Thus, GelMA/POM significantly promotes osteogenesis (Figures 4 and 5C) under oxidative stress by modulating biological processes (Figure 5D).

Notably, KEGG pathway enrichment analysis suggested that the GelMA/POM hydrogel activated the PI3K-Akt signalling pathway in MC3T3-E1 cells (Figure 5E). We examined the biomolecules and proteins associated with the PI3K/Akt pathway using qRT–PCR assays. We found a significant increase in the levels of β-catenin mRNA, which is a marker of PI3K/Akt pathway activation. Moreover, we found decreased mRNA levels of GSK-3β and PTEN, which are negative regulatory molecules. The above results confirmed that the GelMA/POM hydrogel set activated the PI3K-Akt signalling pathway in MC3T3-E1 cells (Figure 5F). The PI3K-Akt pathway is an intracellular signalling pathway that responds to extracellular signals and promotes metabolism, proliferation, cell survival, growth and angiogenesis. This axis has been found to be involved in bone formation and regeneration.[48] This signalling pathway mainly regulates bone formation and regeneration by participating in the proliferation, migration and osteogenic differentiation of osteoblasts.[49,50] In addition, in the PI3K/Akt signalling pathway, phosphorylated Akt (p-Akt) acts as a signaling molecule that activates downstream target proteins involved in cell growth and differentiation. In contrast, GSK-3β, a negative regulatory molecule of the PI3K /Akt pathway, phosphorylates β-catenin, leading to proteasomal degradation of β-catenin and thus inhibiting cellular transcription. However, p-Akt was found to inhibit GSK3β, promote gene expression for cell proliferation and growth, and facilitate the entry of β-catenin into the nucleus.[51,52]

## In vivo Bone Regeneration of Hydrogel

We further investigated the effect of molybdenum-based injectable hydrogels on the repair of bone defects in diabetic mice. The three groups of hydrogels were examined by routine blood, blood biochemistry and histological analyses to determine whether they affected the health of the animals. Blood analysis of the mice implanted with GelMA or GelMA/POM hydrogels was within the normal range, and there was no significant difference compared with the control group (Supplement Figure 6). This finding might be related to the fact that hydrogel facilitates the migration of osteoblasts to the centre of the defect for propagation and differentiation.[53] To further investigate the biocompatibility of GelMA/POM hydrogels, we performed H&E pathological staining on the heart, liver, spleen, lung, and kidney of mice 1 month after hydrogel implantation (Supplement Figure 7). Long-term in vivo safety evaluation confirms that molybdenum-based injectable hydrogels are not significantly toxic in vivo and have promising potential for diabetic bone regeneration.

Diabetic mice were modelled with distal femoral defects, and the repair of the defects was observed at 2 and 4 weeks (Supplement Figure 8). At 2 and 4 weeks of surgical modelling, mice were euthanized, the distal femoral bone defects were observed using micro-CT, and H&E staining was performed on the defect sites. The data obtained by micro-CT were reconstructed in three dimensions, and the results (Figure 6A) and reconstructed images were observed. The trend of bone regeneration involved growth from the edge of the defect to the centre. Bone defect repair was significantly faster in the GelMA/POM group than in the other groups, especially in the central area of the defect. In addition, the GelMA/POM group possessed higher BMD (Figure 6B) and BV/TV (Figure 6C) values than to the other groups. The degree of bone defect repair in the GelMA/POM hydrogel group was best at both 2 and 4 weeks, indicating that the presence of POM protects cells from oxidative stress damage during all stages of bone regeneration. This finding was attributed to the sustained release of POM from the nanohydrogels.

In addition, new bone formation was detected by histological analysis after H&E staining at 2 weeks and 4 weeks (Figure 7). Based on the results of the histological analysis, we found that the GelMA/POM group had more new bone and fibrous tissue. This result is due to the presence of the ROS scavenger POM; cells avoid oxidative stress damage and have better biological capacity and bone formation.[54] Therefore, the GelMA/POM hydrogel is a promising bone repair filler to promote diabetic bone regeneration.

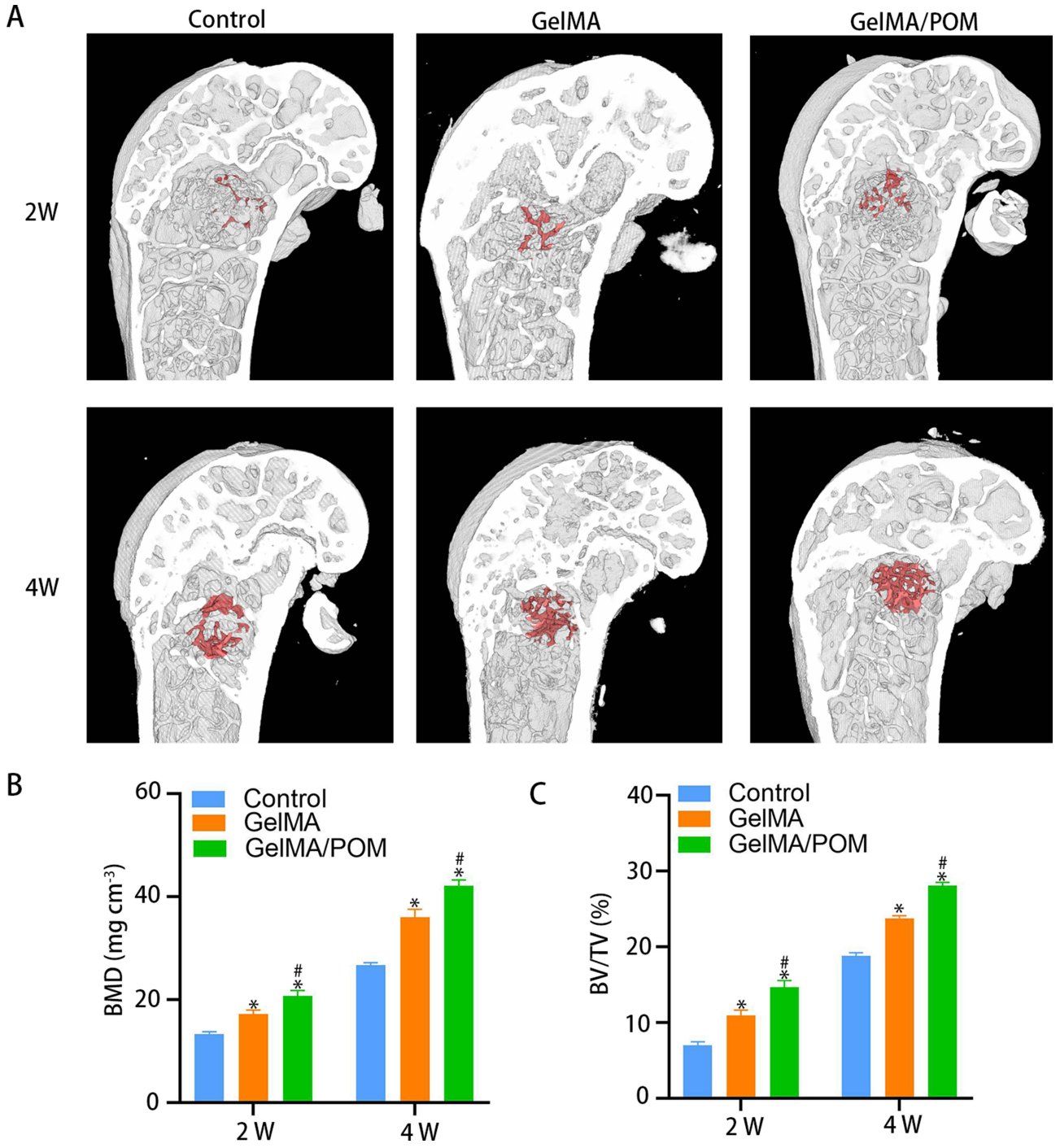


**Figure 6** The osteogenesis properties of hydrogel in vivo. (**A**) 3D reconstructed images showing the effects of different hydrogel on the new bone tissue formation inside the defect site. The bone defect area was circled by red shading. (**B**) Bone mineral density at 2 and 4 weeks. (n = 3, each group). (**C**) Bone volume fraction at 2 and 4 weeks. (*And #Indicate $p < 0.05$ in comparison with Control group and GelMA group, respectively.).

In summary, GelMA/POM hydrogels promote osteogenesis and bone regeneration by scavenging ROS, which corroborates the results of in vitro experiments and provides a promising approach for diabetic bone regeneration. On the one hand, GelMA/POM achieves sustained release of POM, which alters its valence state to resist oxidative stress generated by ROS in a time frame commensurate with bone regeneration. On the other hand, the role of GelMA/POM in promoting bone regeneration may be related to activation of the PI3K/Akt signalling pathway. Furthermore, GelMA/

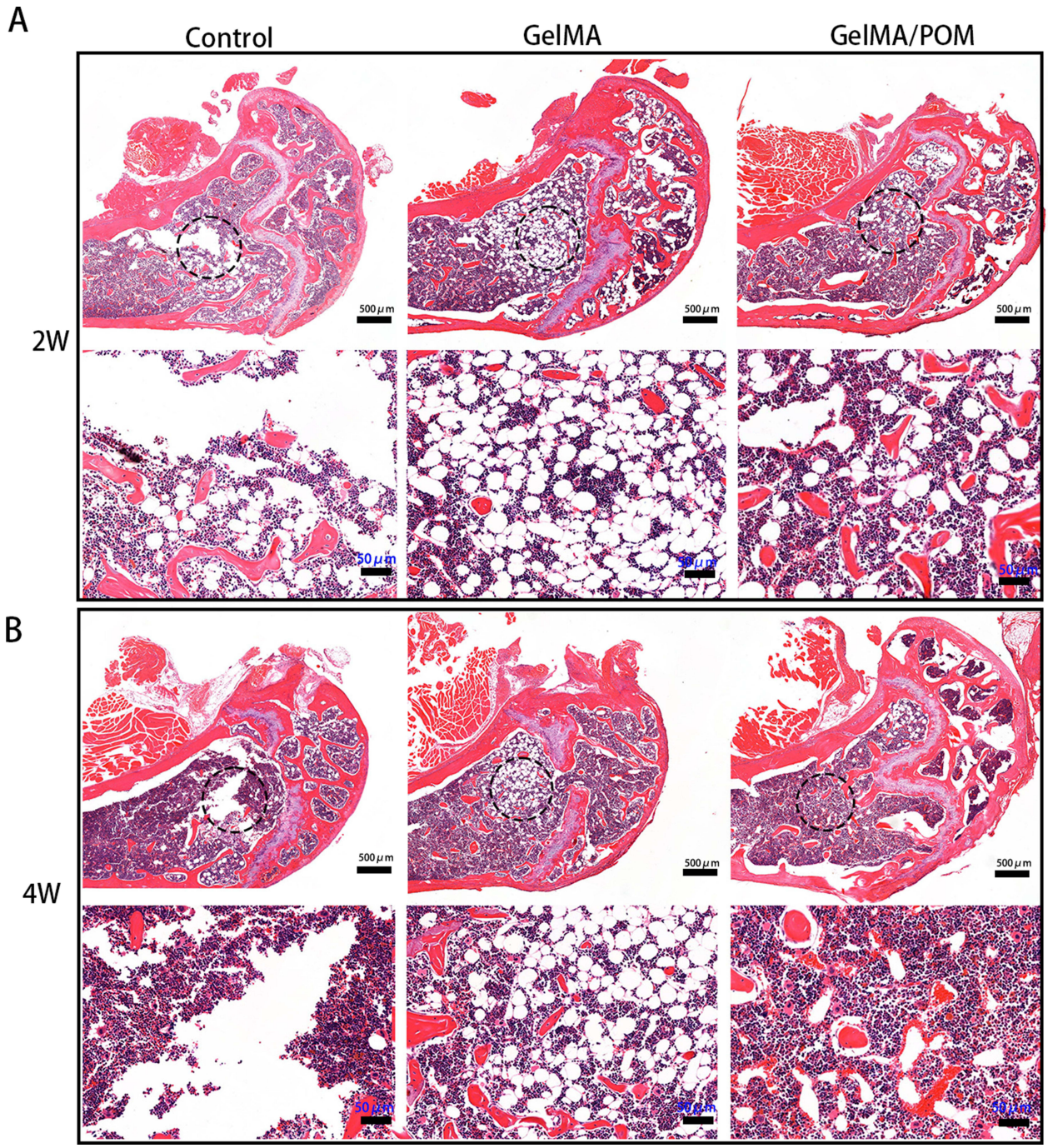


**Figure 7** Histomorphological analysis of newly formed tissue by hematoxylin-eosin staining. Images of HE staining in the distal femur defect area at 2 weeks (**A**) and 4 weeks (**B**) postoperatively.

POM hydrogels have little systemic toxicity compared to conventional systemic administration, as most of the hydrogel is confined to bone tissue and gradually metabolized by the body.

## Conclusion

In this study, we successfully constructed hydrogels with injectability, antioxidant properties and tuned microenvironment of diabetic bone defects by loading POM on the hydrogels. The presence of POM in hydrogels and the scavenging of ROS by POM by changing its valence protect osteoblasts from high ROS levels and thus promote bone formation. In addition,

we found that nanohydrogels can modulate the P13K/Akt signalling pathway to promote osteogenic differentiation under oxidative stress. However, the metabolism of POM in the human body needs further study. In conclusion, GelMA/POM hydrogel innovatively shows promise for the treatment of diabetic bone defects by adjusting the microenvironment.

## Funding

This study was supported by the Research Startup Fund of the Southern University of Science and Technology (Y01416214).

## Disclosure

Dr Xiyu Cai reports grants from the basic and applied research project of Zhuhai science and technology innovation Bureau, during the conduct of the study. The authors report no other conflicts of interest in this study.

## References

1. Ceriello A, Monnier L, Owens D. Glycaemic variability in diabetes: clinical and therapeutic implications. *Lancet Diabetes Endocrinol*. 2019;7(3):221–230. doi:10.1016/S2213-8587(18)30136-0
2. de Oliveira P, Bonfante EA, Bergamo ETP, et al. Obesity/metabolic syndrome and diabetes mellitus on peri-implantitis. *Trends Endocrinol Metab*. 2020;31(8):596–610. doi:10.1016/j.tem.2020.05.005
3. Zhang ZY, Miao LF, Qian LL, et al. Molecular mechanisms of glucose fluctuations on diabetic complications. *Front Endocrinol*. 2019;10:640. doi:10.3389/fendo.2019.00640
4. Ceriello A, Kilpatrick ES. Glycemic variability: both sides of the story. *Diabetes Care*. 2013;36(Suppl 2):S272–5. doi:10.2337/dcS13-2030
5. Qiu P, Li M, Chen K, et al. Periosteal matrix-derived hydrogel promotes bone repair through an early immune regulation coupled with enhanced angio- and osteogenesis. *Biomaterials*. 2020;227:119552. doi:10.1016/j.biomaterials.2019.119552
6. Napoli N, Chandran M, Pierroz DD, Abrahamsen B, Schwartz AV, Ferrari SL. Mechanisms of diabetes mellitus-induced bone fragility. *Nat Rev Endocrinol*. 2017;13(4):208–219. doi:10.1038/nrendo.2016.153
7. Lecka-Czernik B. Diabetes, bone and glucose-lowering agents: basic biology. *Diabetologia*. 2017;60(7):1163–1169. doi:10.1007/s00125-017-4269-4
8. Wu YY, Xiao E, Graves DT. Diabetes mellitus related bone metabolism and periodontal disease. *Int J Oral Sci*. 2015;7(2):63–72. doi:10.1038/ijos.2015.2
9. Li D, Chen K, Tang H, et al. A logic-based diagnostic and therapeutic hydrogel with multistimuli responsiveness to orchestrate diabetic bone regeneration. *Adv Mater*. 2022;34(11):e2108430. doi:10.1002/adma.202108430
10. Yao Y, Zhang H, Wang Z, et al. Reactive oxygen species (ROS)-responsive biomaterials mediate tissue microenvironments and tissue regeneration. *J Mater Chem B*. 2019;7(33):5019–5037. doi:10.1039/C9TB00847K
11. Dulany K, Hepburn K, Goins A, Allen JB. In vitro and in vivo biocompatibility assessment of free radical scavenging nanocomposite scaffolds for bone tissue regeneration. *J Biomed Mater Res A*. 2020;108(2):301–315. doi:10.1002/jbm.a.36816
12. Li J, Wang Q, Yang R, et al. BMI-1 mediates estrogen-deficiency-induced bone loss by inhibiting reactive oxygen species accumulation and T cell activation. *J Bone Miner Res*. 2017;32(5):962–973. doi:10.1002/jbmr.3059
13. Liu Y, Wang C, Wang G, et al. Loureirin B suppresses RANKL-induced osteoclastogenesis and ovariectomized osteoporosis via attenuating NFATc1 and ROS activities. *Theranostics*. 2019;9(16):4648–4662. doi:10.7150/thno.35414
14. Ho-Shui-Ling A, Bolander J, Rustom LE, Johnson AW, Luyten FP, Picart C. Bone regeneration strategies: engineered scaffolds, bioactive molecules and stem cells current stage and future perspectives. *Biomaterials*. 2018;180:143–162. doi:10.1016/j.biomaterials.2018.07.017
15. Bharadwaz A, Jayasuriya AC. Recent trends in the application of widely used natural and synthetic polymer nanocomposites in bone tissue regeneration. *Mater Sci Eng C Mater Biol Appl*. 2020;110:110698. doi:10.1016/j.msec.2020.110698
16. Liu T, Xiao B, Xiang F, et al. Ultrasmall copper-based nanoparticles for reactive oxygen species scavenging and alleviation of inflammation related diseases. *Nat Commun*. 2020;11(1):2788. doi:10.1038/s41467-020-16544-7
17. Tam RY, Yockell-Lelièvre J, Smith LJ, et al. Rationally designed 3D hydrogels model invasive lung diseases enabling high-content drug screening. *Adv Mater*. 2019;31(7):e1806214. doi:10.1002/adma.201806214
18. Ni D, Jiang D, Kutyreff CJ, et al. Molybdenum-based nanoclusters act as antioxidants and ameliorate acute kidney injury in mice. *Nat Commun*. 2018;9(1):5421. doi:10.1038/s41467-018-07890-8
19. Li S, Jiang D, Ehlerding EB, et al. Intrathecal administration of nanoclusters for protecting neurons against oxidative stress in cerebral ischemia/reperfusion injury. *ACS Nano*. 2019;13(11):13382–13389. doi:10.1021/acsnano.9b06780
20. Shi G, Jiang H, Yang F, et al. NIR-responsive molybdenum (Mo)-based nanoclusters enhance ROS scavenging for osteoarthritis therapy. *Pharmacol Res*. 2023;192:106768. doi:10.1016/j.phrs.2023.106768
21. Chen L, Yu C, Xiong Y, et al. Multifunctional hydrogel enhances bone regeneration through sustained release of stromal cell-derived factor-1α and exosomes. *Bioact Mater*. 2023;25:460–471. doi:10.1016/j.bioactmat.2022.07.030
22. Liu T, Weng W, Zhang Y, Sun X, Yang H. Applications of Gelatin Methacryloyl (GelMA) hydrogels in microfluidic technique-assisted tissue engineering. *Molecules*. 2020;26(1):25. doi:10.3390/molecules26010025
23. Nichol JW, Koshy ST, Bae H, Hwang CM, Yamanlar S, Khademhosseini A. Cell-laden microengineered gelatin methacrylate hydrogels. *Biomaterials*. 2010;31(21):5536–5544. doi:10.1016/j.biomaterials.2010.03.064
24. Guo S, Ren Y, Chang R, et al. Injectable self-healing adhesive chitosan hydrogel with antioxidative, antibacterial, and hemostatic activities for rapid hemostasis and skin wound healing. *ACS Appl Mater Interfaces*. 2022;14(30):34455–34469. doi:10.1021/acsami.2c08870
25. Cha GD, Lee WH, Sunwoo SH, et al. Multifunctional injectable hydrogel for in vivo diagnostic and therapeutic applications. *ACS Nano*. 2022;16(1):554–567. doi:10.1021/acsnano.1c07649

26. Liu X, Chen M, Luo J, et al. Immunopolarization-regulated 3D printed-electrospun fibrous scaffolds for bone regeneration. *Biomaterials*. 2021;276:121037. doi:10.1016/j.biomaterials.2021.121037
27. Zhao SJ, Kong FQ, Jie J, et al. Macrophage MSR1 promotes BMSC osteogenic differentiation and M2-like polarization by activating PI3K/AKT/GSK3β/β-catenin pathway. *Theranostics*. 2020;10(1):17–35. doi:10.7150/thno.36930
28. Kaptay G. On the size and shape dependence of the solubility of nano-particles in solutions. *Int J Pharm*. 2012;430(1–2):253–257. doi:10.1016/j.ijpharm.2012.03.038
29. Zhang C, Bu W, Ni D, et al. A polyoxometalate cluster paradigm with self-adaptive electronic structure for acidity/reducibility-specific photothermal conversion. *J Am Chem Soc*. 2016;138(26):8156–8164. doi:10.1021/jacs.6b03375
30. Wang L, Shen M, Hou Q, Wu Z, Xu J, Wang L. 3D printing of reduced glutathione grafted gelatine methacrylate hydrogel scaffold promotes diabetic bone regeneration by activating PI3K/Akt signaling pathway. *Int J Biol Macromol*. 2022;222:1175–1191. doi:10.1016/j.ijbiomac.2022.09.236
31. Bassu G, Laurati M, Fratini E. Microgel dynamics within the 3D porous structure of transparent PEG hydrogels. *Colloids Surf B Biointerfaces*. 2023;221:112938. doi:10.1016/j.colsurfb.2022.112938
32. Divband B, Aghazadeh M, Al-Qaim ZH, et al. Bioactive chitosan biguanidine-based injectable hydrogels as a novel BMP-2 and VEGF carrier for osteogenesis of dental pulp stem cells. *Carbohydr Polym*. 2021;273:118589. doi:10.1016/j.carbpol.2021.118589
33. Ying Y, Huang Z, Tu Y, et al. A shear-thinning, ROS-scavenging hydrogel combined with dental pulp stem cells promotes spinal cord repair by inhibiting ferroptosis. *Bioact Mater*. 2023;22:274–290. doi:10.1016/j.bioactmat.2022.09.019
34. Yan ZY, Zhu JH, Liu GQ, et al. Feasibility and efficacy of a degradable magnesium-alloy GBR membrane for bone augmentation in a distal bone-defect model in beagle dogs. *Bioinorg Chem Appl*. 2022;2022:4941635. doi:10.1155/2022/4941635
35. Lewin S, Kihlström Burenstam Linder L, Birgersson U, et al. Monetite-based composite cranial implants demonstrate long-term clinical volumetric balance by concomitant bone formation and degradation. *Acta Biomater*. 2021;128:502–513. doi:10.1016/j.actbio.2021.04.015
36. Niu X, Ferracci G, Lin M, et al. Highly substituted decoupled gelatin methacrylamide free of hydrolabile methacrylate impurities: an optimum choice for long-term stability and cytocompatibility. *Int J Biol Macromol*. 2021;167:479–490. doi:10.1016/j.ijbiomac.2020.11.187
37. Kaemmerer E, Melchels FP, Holzapfel BM, Meckel T, Hutmacher DW, Loessner D. Gelatine methacrylamide-based hydrogels: an alternative three-dimensional cancer cell culture system. *Acta Biomater*. 2014;10(6):2551–2562. doi:10.1016/j.actbio.2014.02.035
38. Zhou J, Li XY, Liu YJ, et al. Full-coverage regulations of autophagy by ROS: from induction to maturation. *Autophagy*. 2022;18(6):1240–1255. doi:10.1080/15548627.2021.1984656
39. Casati L, Pagani F, Maggi R, Ferrucci F, Sibilia V. Food for bone: evidence for a role for delta-tocotrienol in the physiological control of osteoblast migration. *Int J Mol Sci*. 2020;22(1):21. doi:10.3390/ijms22010021
40. Zhou XY, Xu XM, Wu SY, et al. Low-intensity pulsed ultrasound promotes spinal fusion and enhances migration and proliferation of MG63s through sonic hedgehog signaling pathway. *Bone*. 2018;110:47–57. doi:10.1016/j.bone.2018.01.025
41. Liang Q, Du L, Zhang R, Kang W, Ge S. Stromal cell-derived factor-1/Exendin-4 cotherapy facilitates the proliferation, migration and osteogenic differentiation of human periodontal ligament stem cells in vitro and promotes periodontal bone regeneration in vivo. *Cell Prolif*. 2021;54(3):e12997. doi:10.1111/cpr.12997
42. Debnath S, Yallowitz AR, McCormick J, et al. Discovery of a periosteal stem cell mediating intramembranous bone formation. *Nature*. 2018;562(7725):133–139. doi:10.1038/s41586-018-0554-8
43. Li G, Jian Z, Wang H, Xu L, Zhang T, Song J. Irisin promotes osteogenesis by modulating oxidative stress and mitophagy through SIRT3 signaling under diabetic conditions. *Oxid Med Cell Longev*. 2022;2022:3319056. doi:10.1155/2022/3319056
44. Lin Z, He H, Wang M, Liang J. MicroRNA-130a controls bone marrow mesenchymal stem cell differentiation towards the osteoblastic and adipogenic fate. *Cell Prolif*. 2019;52(6):e12688. doi:10.1111/cpr.12688
45. Fan T, Qu R, Yu Q, et al. Bioinformatics analysis of the biological changes involved in the osteogenic differentiation of human mesenchymal stem cells. *J Cell Mol Med*. 2020;24(14):7968–7978. doi:10.1111/jcmm.15429
46. Sefkow-Werner J, Machillot P, Sales A, et al. Heparan sulfate co-immobilized with cRGD ligands and BMP2 on biomimetic platforms promotes BMP2-mediated osteogenic differentiation. *Acta Biomater*. 2020;114:90–103. doi:10.1016/j.actbio.2020.07.015
47. Yan CP, Wang XK, Jiang K, et al. β-Ecdysterone enhanced bone regeneration through the BMP-2/SMAD/RUNX2/Osterix signaling pathway. *Front Cell Dev Biol*. 2022;10:883228. doi:10.3389/fcell.2022.883228
48. Sun K, Luo J, Guo J, Yao X, Jing X, Guo F. The PI3K/AKT/mTOR signaling pathway in osteoarthritis: a narrative review. *Osteoarthritis Cartilage*. 2020;28(4):400–409. doi:10.1016/j.joca.2020.02.027
49. Tang L, Wu M, Lu S, et al. Fgf9 negatively regulates bone mass by inhibiting osteogenesis and promoting osteoclastogenesis via MAPK and PI3K / AKT Signaling. *J Bone Miner Res*. 2021;36(4):779–791. doi:10.1002/jbmr.4230
50. Abdurahman A, Li X, Li J, et al. Loading-driven PI3K/Akt signaling and erythropoiesis enhanced angiogenesis and osteogenesis in a post-menopausal osteoporosis mouse model. *Bone*. 2022;157:116346. doi:10.1016/j.bone.2022.116346
51. Shen M, Wang L, Feng L, et al. bFGF-loaded mesoporous silica nanoparticles promote bone regeneration through the Wnt/β-Catenin signalling pathway. *Int J Nanomedicine*. 2022;17:2593–2608. doi:10.2147/IJN.S366926
52. Yang C, Liu X, Zhao K, et al. miRNA-21 promotes osteogenesis via the PTEN/PI3K/Akt/HIF-1α pathway and enhances bone regeneration in critical size defects. *Stem Cell Res Ther*. 2019;10(1):65. doi:10.1186/s13287-019-1168-2
53. Zhang X, Huang P, Jiang G, et al. A novel magnesium ion-incorporating dual-crosslinked hydrogel to improve bone scaffold-mediated osteogenesis and angiogenesis. *Mater Sci Eng C Mater Biol Appl*. 2021;121:111868. doi:10.1016/j.msec.2021.111868
54. Zhao B, Peng Q, Wang D, et al. Leonurine protects bone mesenchymal stem cells from oxidative stress by activating mitophagy through PI3K/Akt/mTOR pathway. *Cells*. 2022;12(1):11. doi:10.3390/cells12010011